PAPER

Check for updates

External stimuli responsive syneresis of amino acid-based bioactive hydrogels: a sustainable platform for environmental remediation†

Abhinandan Bera,[a] Ritu Raj Patel,[b] S. Daisy Precilla,[c] Meenakshi Singh, [ID][b] B. Agiesh Kumar,[c] Sudipta Bhowmik, [ID][cd] Mayank Varshney[e] and Subhasish Roy [ID] *[a]

Syneresis of hydrogels in the presence of external stimuli has potential applications in waste-water treatment and water purification. Fmoc-3-(1-naphthyl)-L-alanine (**Fmoc-¹Nap-A**) and Fmoc-3-(2-naphthyl)-L-alanine (**Fmoc-²Nap-A**) form stable hydrogels in 50 mM phosphate buffer of pH 7.4 with minimum gelation concentrations (MGCs) 0.0455% (w/v) and 0.0375% (w/v) respectively. This is the first report on hydrogelation of **Fmoc-¹Nap-A** and **Fmoc-²Nap-A** in phosphate buffer at physiological pH and their external stimuli-responsive syneresis. **Fmoc-¹Nap-A** and **Fmoc-²Nap-A** are found to be biocompatible and exhibit potent anti-bacterial activity. **Fmoc-¹Nap-A** shows anticancer activity towards the pancreatic cancer cell line, PANC-1 cells. Syneresis of **Fmoc-¹Nap-A** and **Fmoc-²Nap-A** hydrogels has been studied in the presence of various toxic metal ions and the thioflavin T dye. The hydrogel obtained from **Fmoc-¹Nap-A** shows syneresis in the presence of Hg^{II} and Ni^{II} ions selectively and also in the presence of the thioflavin T (**TT**) dye; however, the hydrogel obtained from **Fmoc-²Nap-A** shows syneresis only in the presence of the thioflavin T (**TT**) dye. Structural, mechanical, and morphological characterization have been performed by using X-ray powder diffraction, FT-IR, rheology, and FE-SEM analyses. Interestingly, the absorption of the **TT** dye from water is more efficient for **Fmoc-²Nap-A** compared to **Fmoc-¹Nap-A**. Various spectroscopic experiments have been carried out to estimate the absorption capacity for toxic metal ions and also the **TT** dye. Minimum amounts of 3.14 mM of 0.6 mL of Hg^{II} ions, 4.21 mM of 0.3 mL Ni^{II} ions and 3.14 mM of 0.1 mL of the **TT** dye for **Fmoc-¹Nap-A** and 3.1361 mM of 0.2 mL of the **TT** dye for **Fmoc-²Nap-A** are at least required to be added on top of 2 mL of 0.08% w/v concentration of hydrogels to exhibit syneresis. The absorption capacities for the **TT** dye are estimated to be 912.51 μg and 981.92 μg from 1000 μg of **TT** dye solution by 2 mL of **Fmoc-¹Nap-A** and **Fmoc-²Nap-A** hydrogels respectively at a concentration of 0.08% w/v (1600 μg gelator molecules) each by using UV-Vis spectroscopy. ICP-MS data also reveal that 2 mL of the **Fmoc-¹Nap-A** gel is capable of removing 208.29 μg of Hg^{II} ions from a total of 440.61 μg of Hg^{II} contaminated water after syneresis. These hydrogels are capable of removing toxic heavy metal ions (Hg^{II}) and toxic dye (**TT**) selectively from waste-water sustainably, showing applicability in the field of water research for environmental remediation.

[a] *Department of Chemistry, Birla Institute of Technology and Science-Pilani, K K Birla Goa Campus, NH 17B, Zuarinagar, Sancoale, Goa 403726, India. E-mail: subhasishr@goa.bits-pilani.ac.in*

[b] *Department of Medicinal Chemistry, Institute of Medicinal Chemistry, Institute of Medical Sciences, Banaras Hindu University, Varanasi 221005, UP, India*

[c] *Mahatma Gandhi Medical Advanced Research Institute (MGMARI), Central Inter-Disciplinary Research Facility (CIDRF), Sri Balaji Vidyapeeth (Deemed to be University), Puducherry, 607402, India*

[d] *Department of Biophysics, Molecular Biology and Bioinformatics, University of Calcutta, 92, A.P.C. Road, Kolkata, 700009, India*

[e] *Senior Application Specialist, Characterization Division, Anton Paar India Pvt. Ltd., Phase V, Udyog Vihar Industrial Area, Gurgaon 122016, Haryana, India*

† Electronic supplementary information (ESI) available. See DOI: https://doi.org/10.1039/d5ma00274e

Introduction

Amino acid-based low-molecular-weight hydrogelators are gaining significant attention globally in the era of modern cutting-edge research due to their versatile applications from bench to bedside.[1–12] The presence of the hydrophilic edge (–COOH, C terminus), hydrophobic edge (protected N-terminus), and appropriate side chains makes the molecules efficient hydrogelators by maintaining a judicious balance of hydrophobicity and hydrophilicity. In the three-dimensional network structures, hydrogelator molecules are bound together through various weak non-covalent interactions including hydrogen

bonding, pi–pi stacking, and van der Waals interaction[13–17] and hold huge amounts of water to form hydrogels. Research on amino acid-based hydrogels extends to the field of tissue engineering,[18] drug delivery systems,[19–24] toxic metal ions and anion sensing,[25–28] dye absorption and toxic metal ion removal,[29–31] nanoparticle and nanocluster syntheses,[32–34] antibacterial agents,[35–38] photoswitching behavior[39] and catalysis.[40–42] Yang and his co-workers have previously reported hydrogelation of Fmoc-3-(2-naphthyl)-D-alanine in aqueous Na₂CO₃ solution and its hybrid hydrogelation within the agarose hydrogel that can remove toxic dyes like methyl violet from aqueous solution.[43] When a gel expels solvent from its three-dimensional cross-linked matrix system, the volume of the gel matrix decreases from its initial volume, called syneresis of the gel.[44] Thus, it is a process of phase-separation from the gel state to a mixture of gel and solution states by excluding solvent from the initial volume of the gel state. Syneresis is a common and natural phenomenon that happens when serum release during blood clotting.[45] The food quality has also been determined by syneresis in various foods including jams, surimi, jellies, sauces, dairy products, tomato juice, meat, and soybean products. Various hydrogels show syneresis by themselves upon aging.[46,47] A different type of hydrogelator that forms a stable hydrogel in the presence of an aqueous buffer and is stable for a long time, however, undergoes shrinking by releasing some water from the hydrogel matrix upon the addition of specific stimuli through absorption followed by co-assembly are known as external stimuli responsive syneresis. The self-shrinking of the hydrogels is comparatively common; however, the external stimuli-induced shrinkage of hydrogels is not yet explored well. The first thermally responsive syneresis effect of supramolecular polymers based on glycosylated amino acid has been reported by the Hamachi research group.[44] They have shown that gels expelled water from the three-dimensional matrix upon application of heat and again upon cooling down the gel swelled to regain its pristine state. In the process of syneresis, hydrogels release water molecules from their three-dimensional network induced by external stimuli, which may be due to the enhanced hydrophobicity at their local network structures by reducing volume compared to the initial stage. Banerjee's group has reported a self-shrinkable low molecular weight, triphenyl alanine-based hydrogel.[47] After forming a stable hydrogel at pH 7.4, it shows syneresis upon aging for 7 days. Syneresis has been used for the removal of toxic metal ions and dye including Pb^II and methylene blue.[47] Ulijn and his research group have reported mechanical contact assisted syneresis of dipeptide diphenylalanine (FF) and its amidated derivative (FF-NH2)-based hydrogels.[48] Liu and co-workers have reported a peptide-based hydrogelator, OGAc (*N*-octadecanoyl-1,5-bis(L-glutamic acid)-L-glutamic diamide), which forms a stable hydrogel in the presence of a wide range of metal ions, and concluded that most of the metal ions triggered the syneresis of the gel.[49] They have observed that with the use of increasing amounts of metal ions in the gel, the syneresis occurs more rapidly.[49] Das and his research group have discovered azobenzene-functionalized short peptide-based stable gel formation in an aqueous medium; however, upon irradiation with UV light (365 nm) the gel exhibited syneresis, and the gel matrix released around 50% of solvent from the matrix.[50] Adams and his research group have investigated the change in the hydrophobicity of the system with the addition of different organic salts and the controlled syneresis property of a peptide-based hydrogel.[51] External stimuli can be any salt,[51] compound,[52] metal ions,[47] pH,[53–55] temperature,[56] UV light[50,56] and mechanical force.[48] As a result, the expelled water may carry hydrogel nanofibers due to leaching. Syneresis of hydrogels is very useful in some research areas, including water purification,[47,50] drug release,[49] biosensing,[55] and microfluidic devices. In addition to amino acid/peptide-based shrinkable hydrogels, some hydrogels are evolved based on other organic molecules and show syneresis upon aging[57–59] or in the presence of external stimuli,[60] which may be due to the increase of local hydrophobicity.

Here, we report stable hydrogel formation by Fmoc-3-(1-naphthyl)-L-alanine (**Fmoc-¹Nap-A**) and Fmoc-3-(2-naphthyl)-L-alanine (**Fmoc-²Nap-A**) in 50 mM phosphate buffer of pH 7.4. The **Fmoc-¹Nap-A** hydrogel exhibits a very interesting syneresis property in the presence of external stimuli including toxic metal ions (Hg^II), Ni^II ions, and thioflavin T (**TT**) toxic dye; however, **Fmoc-²Nap-A** shows syneresis only in the presence of external stimulus, thioflavin T (**TT**) toxic dye. Thus, the isomeric **Fmoc-¹Nap-A** and **Fmoc-²Nap-A** can be distinguished by simple external stimuli induced syneresis by toxic heavy metal ions Hg^II in water and Ni^II ions in water, which is a very unique property. Both **Fmoc-¹Nap-A** and **Fmoc-²Nap-A** are very selective and have not shown any syneresis in the presence of other metal ions including Ag^I, Ba^II, Ca^II, Cd^II, Co^II, Cr^VI, Cu^II, Fe^II, K^I, Mg^II, Na^I, Pb^II and Zn^II. Interestingly, the **TT** dye absorbing capacity of the **Fmoc-²Nap-A** hydrogel is much higher than that of **Fmoc-¹Nap-A**. Spectroscopic investigations suggest that waste-water treatment can be done to obtain pure water as the dye-absorbed hydrogels release clean water after syneresis. Thus, this approach is one of the green, clean, cost-effective and sustainable platforms for environmental remediation indeed. As waste-water contains high concentrations of toxic dyes and heavy metal ions, these **Fmoc-¹Nap-A** and **Fmoc-²Nap-A** hydrogels can be used to treat waste-water samples to get pure water. The syneresis of **Fmoc-¹Nap-A** and **Fmoc-²Nap-A** hydrogels induced by high concentrations of Hg^II ions in contaminated waste-water can be used to distinguish between the two isomers of **Fmoc-¹Nap-A** and **Fmoc-²Nap-A** because **Fmoc-¹Nap-A** only shows syneresis in the presence of the external stimulus of Hg^II ions; however, **Fmoc-²Nap-A** does not show syneresis by the external stimulus like Hg^II ions. In terms of real field applications, it is important for the materials that will be used for water purification to be safe to handle, non-toxic and are capable of killing and removing bacteria. Water born bacteria can also be killed and purified by using such hydrogels. Thus, there is a relation between water purification and biocompatibility and antibacterial activity. Bio-compatible antimicrobial materials attract high interest in terms of environmental remediation for water research. **Fmoc-¹Nap-A** and **Fmoc-²Nap-A** hydrogels are found to be biocompatible and show potent anti-bacterial, antioxidant and anticancer activities. Such kinds of biocompatible hydrogel materials can be used for sustainable water research in the future.

Experimental section

Instrumentation, sample preparation, and method of analysis

Instrumentation techniques, detailed sample preparation procedures, instrumentations and instrumental methods of analysis are discussed in the ESI.†

Materials and methods

Fmoc-3-(1-naphthyl)-L-alanine (**Fmoc-¹Nap-A**) and Fmoc-3-(2-naphthyl)-L-alanine (**Fmoc-²Nap-A**) are purchased from TCI and the thioflavin T dye (molecular weight: 318.87) was purchased from SRL. Dulbecco's modified Eagle's medium (DMEM, catalogue no. AL007S), Trypsin-EDTA solution 10× (catalogue no. TCL070), and phosphate buffered saline (PBS) (catalogue no. TS1006) were purchased from Hi-Media, Mumbai. Fetal Bovine Serum (FBS) (catalogue no. A5256701) was procured from Thermo Fisher Scientific, South America. Penicillin/streptomycin antibiotic solution (catalogue no. A001) was purchased from Hi-Media, Mumbai. All the other chemicals and reagents used in this study were purchased from SRL, Merck, TCI and Thermo Fisher Scientific, South America.

Preparation of hydrogels. 1.6 mg of **Fmoc-¹Nap-A** and **Fmoc-²Nap-A** hydrogelators were taken in screw capped glass vials separately and 2 mL of 50 mM phosphate buffer of pH 7.4 were added to these glass vials. Glass vials were sonicated for 5 minutes and then heated strongly 10 minutes on a hot plate (hot plate temperature: 150 °C). Glass vials containing both **Fmoc-¹Nap-A** and **Fmoc-²Nap-A** hydrogelator solutions were kept at rest at room temperature for 10 minutes to form stable hydrogels.

Preparation of external stimuli for syneresis. Different concentrations of thioflavin T (**TT**) dye solution were prepared by dissolving solid **TT** in Milli Q water. NiCl$_2$·6H$_2$O salt and Hg(OAc)$_2$ salt were also dissolved in Milli Q water to prepare different concentrations of salt solutions. A detailed description is given in the supplementary documents on page S3 (ESI†).

Preparation of xerogels. Xerogels were prepared through lyophilization of hydrogels to get solid powder.

Results and discussion

Hydrogelation studies

Amphiphilic Fmoc-3-(1-naphthyl)-L-alanine (**Fmoc-¹Nap-A**) and Fmoc-3-(2-naphthyl)-L-alanine (**Fmoc-²Nap-A**) undergo self-assembly to form hydrogels in 50 mM phosphate buffer of pH 7.4 separately. Initially, 2 mg of each hydrogelator (**Fmoc-¹Nap-A** and **Fmoc-²Nap-A**) were transferred into two different 5 mL screw-capped glass vials followed by the addition of 2 mL of 50 mM phosphate buffer solution of pH 7.4. After that, the screw-capped glass vials containing the hydrogelators in phosphate buffer were sonicated for 5 minutes followed by heating strongly on a hot plate (at 150 °C for 10 minutes) to dissolve completely and then kept at rest at room temperature. Both **Fmoc-¹Nap-A** and **Fmoc-²Nap-A** form stable hydrogels after 10 minutes. To find the minimum gelation concentrations (MGCs), 200 μL of phosphate buffer solutions at each interval were added into

these hydrogel vials and heated to dissolve followed by keeping them at rest to check whether the formation of the hydrogels is taking place or not. This way the minimum concentration of these hydrogelators in the phosphate solution has been estimated after repeating each hydrogel in three different vials. The minimum gelation concentration (MGC) of **Fmoc-¹Nap-A** is estimated to be 0.0455 ± 0.0007% (w/v) (1.0400 mM) and for **Fmoc-²Nap-A** it is estimated to be 0.0375 ± 0.0023% (w/v) (0.8572 mM). The chemical structures and hydrogels in tilted glass vials of **Fmoc-¹Nap-A** and **Fmoc-²Nap-A** are shown in Fig. 1.

Gel melting temperature (T_{gel}) estimation

To know the thermal stability of these hydrogels (**Fmoc-¹Nap-A** and **Fmoc-²Nap-A**), hydrogels at different concentrations have been prepared for both the hydrogelators. Concentrations of 0.06% (w/v), 0.07% (w/v), 0.08% (w/v), 0.09% (w/v), 0.10% (w/v) and 0.11% (w/v) hydrogels have been used for both **Fmoc-¹Nap-A** and **Fmoc-²Nap-A** for a comparative study.

The melting points of the hydrogels at different concentrations for both **Fmoc-¹Nap-A** and **Fmoc-²Nap-A** have been measured by submerging in a digitally displayed temperature-controlled water bath. At each concentration, three hydrogels at three different glass vials have been prepared and their melting points have been measured. The average melting points at every concentration have been considered for T_{gel} vs. concentration profiles (Fig. 2). The standard deviation error for each concentration has been incorporated (Fig. 2). At each temperature, the hydrogel vials have been kept submerged in the water bath for at least 5 minutes to check the gelation melting points. Fig. 2 shows that the **Fmoc-²Nap-A** hydrogel is thermally more stable than the **Fmoc-¹Nap-A** hydrogel.

Rheological studies

To know the mechanical strength and viscoelastic behavior[61] of the **Fmoc-¹Nap-A** and **Fmoc-²Nap-A** hydrogels at 0.1% (w/v), frequency sweep rheological experiments have been performed. Both the **Fmoc-¹Nap-A** and **Fmoc-²Nap-A** hydrogels' storage moduli (G') are found to be higher than the loss moduli (G'')
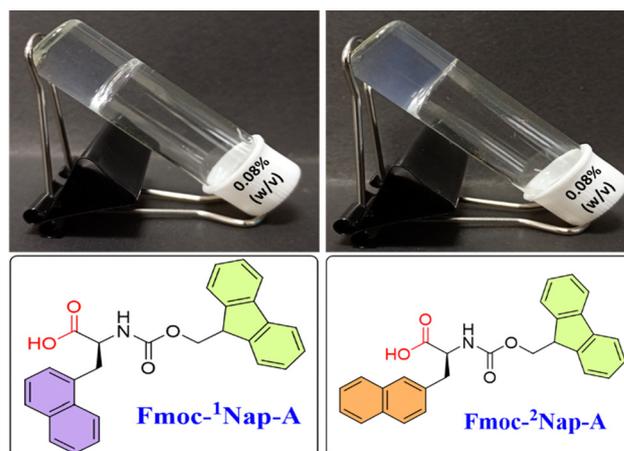

Fig. 1 Chemical structures of Fmoc-3-(1-naphthyl)-L-alanine (**Fmoc-¹Nap-A**) and Fmoc-3-(2-naphthyl)-L-alanine (**Fmoc-²Nap-A**) and hydrogels in tilted glass vials.
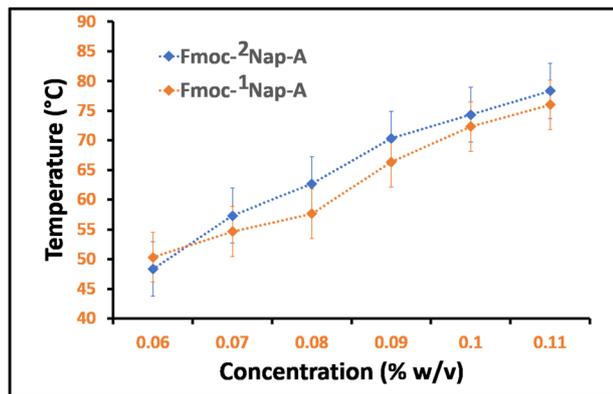
Fig. 2 Concentration dependent T_{gel} profiles of **Fmoc-^{1}Nap-A** and **Fmoc-^{2}Nap-A** hydrogels.

(Fig. 3), indicating the stability of the hydrogels within the studied angular frequency region. Fig. 3 indicates the higher mechanical stability of the **Fmoc-^{2}Nap-A** hydrogel compared to **Fmoc-^{1}Nap-A,** which may be due to the lower MGC value of **Fmoc-^{2}Nap-A** than **Fmoc-^{1}Nap-A.**

UV-Vis spectroscopic study

A UV-Vis absorption spectroscopic study of the hydrogels **Fmoc-^{1}Nap-A** and **Fmoc-^{2}Nap-A** and their dilute solutions has been performed to understand the aggregation behavior of the hydrogels. Absorption maxima (Fig. S1, ESI†) at 265 nm have been observed for both **Fmoc-^{1}Nap-A** and **Fmoc-^{2}Nap-A** hydrogels. A decrease in absorption intensities with no shift in absorption maxima has been observed for gel to sol transition upon dilution, indicating a higher scattering effect and absorption from the higher order aggregates (Fig. S1, ESI†) for both the hydrogels compared to their diluted solution states.[62,63]

Fluorescence spectroscopic study

A fluorescence spectroscopic study of **Fmoc-^{1}Nap-A** and **Fmoc-^{2}Nap-A** hydrogels below their MGCs at various dilutions has been performed. **Fmoc-^{1}Nap-A** shows emission maxima at

Fig. 3 Rheological frequency sweep profile as a function of storage modulus (G') and loss modulus (G'') for **Fmoc-^{1}Nap-A** and **Fmoc-^{2}Nap-A** hydrogels.

337 nm; however, **Fmoc-^{2}Nap-A** shows fluorescence emission maxima at 336 nm upon excitation at a wavelength of 265 nm (Fig. S2, ESI†). Upon dilution from 918.45 μM hydrogel aggregated solutions it has been found that initially fluorescence intensity started to increase for 457.14 μM and 304.76 μM solutions and then gradually started to decrease upon dilution for both the hydrogels (Fig. S2, ESI†). Overall, the fluorescence intensities have been enhanced upon dilution compared to their concentrated solutions up to a certain concentration of dilutions. The enhancement of fluorescence emission intensities suggests higher ordered aggregation[62,63] in their self-assembled states.

Structural studies

FT-IR study. Fourier transform infrared (FT-IR) spectroscopic studies have been performed for **Fmoc-^{1}Nap-A** and **Fmoc-^{2}Nap-A** in their bulk states as well as in their xerogel states on KBr pellets. Significant peaks have been found at 3319.49 cm^{-1} (strong) for N–H stretching frequency for the amide bond, 1705.07 cm^{-1} (strong) for carbonyl stretching frequency for the amide bond, 1529.55 cm^{-1} (strong) for N–H bending frequency and a very weak peak at 1598.98 cm^{-1} for C=C stretching frequency of the aromatic ring for the **Fmoc-^{1}Nap-A** bulk solid (Fig. S3 and Table S1, ESI†). Significant peaks at 3317.56 cm^{-1} (strong) due to N–H stretching frequency for the amide bond, 1691.57 cm^{-1} (strong) for carbonyl stretching frequency for the amide group, 1533.40 cm^{-1} (strong) for N–H bending of the amide group and a very weak peak at 1600.91 cm^{-1} for C=C stretching frequency of the aromatic group for the **Fmoc-^{2}Nap-A** bulk solid have been observed. The **Fmoc-^{1}Nap-A** xerogel shows characteristic peaks at 3334.92 cm^{-1}, 1691.57 cm^{-1} and 1535.33 cm^{-1} for N–H stretching of the amide bond, carbonyl stretching of the amide bond and N–H bending of the amide bond respectively. The **Fmoc-^{2}Nap-A** xerogel shows significant peaks at 3379.28 cm^{-1}, 1691.57 cm^{-1}, and 1535.33 cm^{-1} for NH stretching of the amide bond, carbonyl stretching of the amide bond and N–H bending of the amide bond respectively. It has been understood from the significant changes in their peak positions for **Fmoc-^{1}Nap-A** and **Fmoc-^{2}Nap-A** xerogels compared to their native bulk solid that due to the involvement of hydrogen bonding interaction hydrogel formation has been observed (Fig. S3, ESI†) for both the hydrogelators.

X-ray diffraction study

To investigate the molecular packing arrangements and the involvement of various non-covalent interactions in supramolecular hydrogelation, X-ray diffraction analysis has been performed. Molecular lengths for **Fmoc-^{1}Nap-A** and **Fmoc-^{2}Nap-A** have been found at 17.03 Å and 17. 97 Å (at a lower energy state obtained from ChemDraw 3D) respectively. Both hydrogelators, **Fmoc-^{1}Nap-A** and **Fmoc-^{2}Nap-A,** formed anti-parallel beta-sheet-like structures in their hydrogel states. Peaks at a d-spacing of 4.61 Å ($2\theta = 19.22°$) represent the distance between two adjacent beta-strands and a d-spacing value of 9.33 Å ($2\theta = 9.47°$) represents the distance between two neighbouring layers of the beta-sheet for **Fmoc-^{1}Nap-A** (Fig. 4). The peak at a
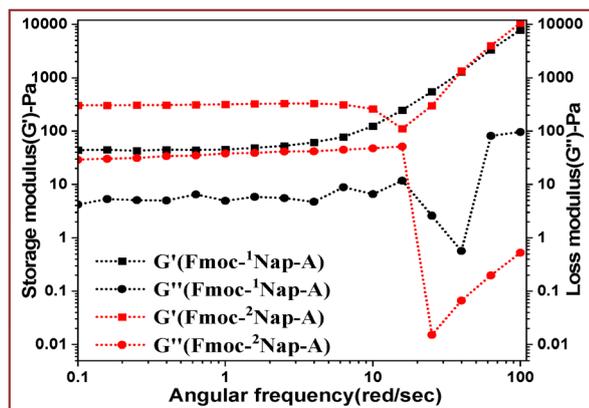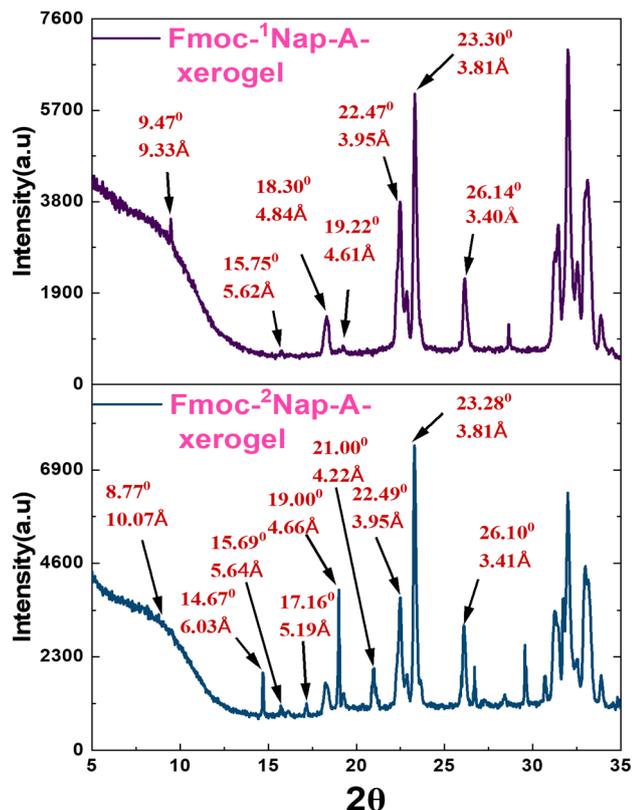
Fig. 4 X-ray powder diffraction patterns of the **Fmoc-¹Nap-A** and **Fmoc-²Nap-A** xerogels.

Fig. 5 FE-SEM images of the **Fmoc-¹Nap-A** and **Fmoc-²Nap-A** hydrogels in their dried gel forms.

d-spacing value of 4.66 Å ($2\theta = 19.00°$) represents the distance between two adjacent beta strands and that at a *d*-spacing value of 10.07 Å ($2\theta = 8.77°$) represents the distance between two neighbouring layers of the beta-sheet for **Fmoc-²Nap-A** (Fig. 4). Both the hydrogelators' (**Fmoc-¹Nap-A** and **Fmoc-²Nap-A**) pi–pi stacking interaction peaks in their xerogel states have appeared at a *d*-spacing of 3.81 Å. Both the hydrogelators have formed lamellar structures in their self-assembled hydrogel states due to the presence of peaks at $D/2$, $D/3$, $D/4$, and $D/5$ respectively (D obtained from ChemDraw 3D at their lower energy states) (Table S2, ESI†).

Morphology study

The FE-SEM experiment has been performed to understand the morphological characteristics of **Fmoc-¹Nap-A** and **Fmoc-²Nap-A** in their hydrogel states. Cross-linked nanofibrillar network structures have been found for both **Fmoc-¹Nap-A** and **Fmoc-²-Nap-A** hydrogels. Also, it has been found that the nanofiber density of **Fmoc-²Nap-A** is more compared to that of **Fmoc-¹-Nap-A**. The average diameter has been estimated to be 8.77 ± 1.21 nm and 11.698 ± 3 nm for **Fmoc-¹Nap-A** and **Fmoc-²Nap-A** in their hydrogel states (Fig. 5) respectively. Entangled nanofibrillar morphology for both **Fmoc-¹Nap-A** and **Fmoc-²Nap-A** hydrogels has also been obtained from a high resolution transmission electron microscopic (HR-TEM) imaging study (Fig. S4, ESI†).

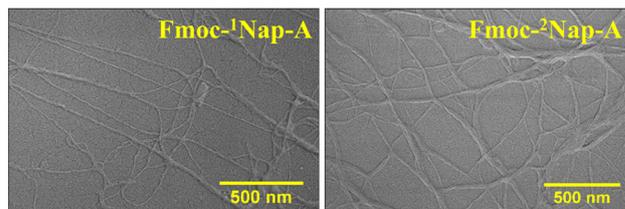FE-SEM images reveal the presence of more cross-linked nanofibrillar morphology for the **Fmoc-²Nap-A** hydrogel compared to **Fmoc-¹Nap-A** hydrogel. This suggests stronger hydrogel formation for **Fmoc-²Nap-A** compared to **Fmoc-¹Nap-A** hydrogel at the same concentration [0.1% (w/v)] which has also evident from rheological measurements. This could also be due to the higher MGC of the **Fmoc-¹Nap-A** hydrogel compared to that of the **Fmoc-²Nap-A** hydrogel.

Syneresis of hydrogels in the presence of toxic metal ions

Various metal ion aqueous solutions including Ag^I, Na^I, K^I, Cu^{II}, Ni^{II}, Ca^{II}, Zn^{II}, Cd^{II}, Pb^{II}, Hg^{II}, Ba^{II}, Mg^{II} and Fe^{II} have been added on top of both the **Fmoc-¹Nap-A** and **Fmoc-²Nap-A** hydrogels to investigate external stimuli induced syneresis. Interestingly, the **Fmoc-¹Nap-A** hydrogel shows syneresis in the presence of Ni^{II} and Hg^{II} metal ions; however, **Fmoc-²Nap-A** did not show syneresis in the presence of a series of metal ions used for syneresis. The effects of concentrations and volume of the external stimuli have been investigated to know the critical concentrations and volume required for the syneresis.

Concentration dependent syneresis in the presence of Hg^{II} and Ni^{II} ions. In this experiment, 2 mL of the **Fmoc-¹Nap-A** hydrogel at 0.08% w/v has been taken in four different glass vials, and 1 mL of Hg^{II} ions at various concentrations including 1 mg mL^{-1}, 0.1 mg mL^{-1}, 0.01 mg mL^{-1} and 0.001 mg mL^{-1} has been added on top of the four different hydrogel glass vials. It has been found that the **Fmoc-¹Nap-A** hydrogel shows syneresis, where 1 mL of 1 mg mL^{-1} of Hg^{II} toxic metal ion solution has been added. However, other vials did not show any syneresis. A similar experiment has been performed for Ni^{II} metal ions and the exactly same results have been found, which means 1 mg of Hg^{II} and 1 mg of Ni^{II} metal ions in 1 mL of Milli Q water must be separately added on top of 2 mL of **Fmoc-¹Nap-A** hydrogels at 0.08% w/v concentration for syneresis and below this concentration, no syneresis has been observed (Fig. 6).

A control experiment has been performed with Milli Q water for comparison with Hg^{II} and Ni^{II} metal ion solutions to determine whether the syneresis happened only in the presence of these salt solutions or it happened in the presence of water only (Fig. S5, ESI†). In this experiment, 2 mL (0.08% w/v) of the **Fmoc-¹Nap-A** hydrogel has been taken in three different vials. 1 mL of Hg^{II} and Ni^{II} metal ion solutions and 1 mL of Milli Q water have been added on top on these three **Fmoc-¹Nap-A** hydrogel vials. Vials were kept undisturbed for three days. It has been found that syneresis has been observed in the vials with Hg^{II} and Ni^{II} metal ions. However, dissolution of the hydrogelators has been observed for all these systems as evident from the UV-Vis spectroscopic study (Fig. S6, ESI†). The amount of
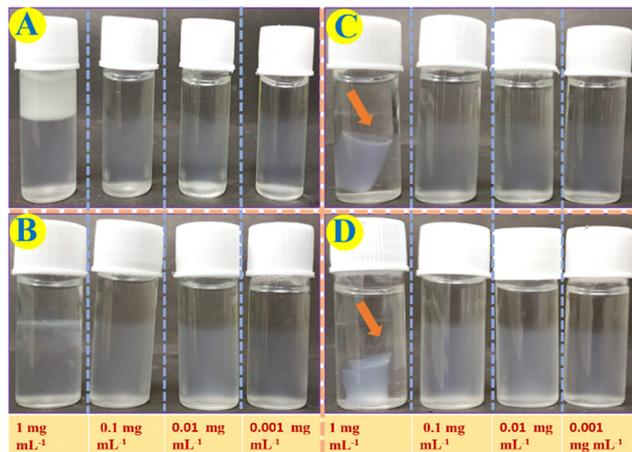
Fig. 6 Concentration dependent syneresis of the **Fmoc-¹Nap-A** hydrogels at different time intervals including just after addition for (A) Hg^{II} metal ions and (B) Ni^{II} metal ions and after 3 days from the addition for (C) Hg^{II} metal ions and (D) Ni^{II} metal ions. Concentrations of the metal ions added at a volume of 1 mL are mentioned at the bottom of the figure.
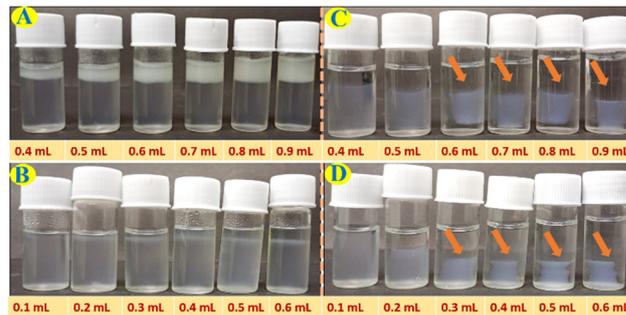

Fig. 7 Volume dependent syneresis of different metal ions added on top of the **Fmoc-¹Nap-A** hydrogel at different time intervals including just after addition for (A) Hg^{II} and (B) Ni^{II} metal ions and after 3 days from the addition for (C) Hg^{II} and (D) Ni^{II} metal ions. Volume of the metal ions added is mentioned at the bottom of each vial at a concentration of 1 mg mL^{-1}.

hydrogelator dissolution happened after 3 days for these three glass vials has been estimated using a standard calibration curve (Fig. S7, ESI†), Fig. S6 and Table S3 (ESI†).

Volume dependent syneresis in the presence of Hg^{II} and Ni^{II} ions. Two different stock solutions of Hg^{II} and Ni^{II} metal salts at 1 mg mL^{-1} concentration have been prepared to check the effect of volume on syneresis as syneresis happened in the presence of Hg^{II} and Ni^{II} metal salt solutions at 1 mg mL^{-1} concentration. It has been found that upon increasing the volume of Hg^{II} metal ions, syneresis happened significantly. 0.1 mL, 0.2 mL, 0.3 mL, 0.4 mL, 0.5 mL, and 0.6 mL of Ni^{II} metal ion stock solutions have been added on top of the six different vials containing 2 mL of the **Fmoc-¹Nap-A** hydrogel separately at 0.08% w/v concentration. 0.3 mL volume and more of Ni^{II} and 0.6 mL and more of Hg^{II} metal ion stock solutions of concentration 1 mg mL^{-1} have been required for syneresis to happen (Fig. 7).

ICP-MS analysis

Percent removal capacity of Hg^{II} ions from Hg^{II} ions contaminated water by the **Fmoc-¹Nap-A** hydrogel has been estimated by using ICP-MS analysis on the released water part after the Hg^{II} ions induced syneresis of the hydrogel. Estimation of % removal of the Hg^{II} ions from the contaminated water by the **Fmoc-¹Nap-A** hydrogel has been shown in Table S4 and Fig. S8 (ESI†). It has been found that due to syneresis (Fig. S8, ESI†), the **Fmoc-¹Nap-A** hydrogel is capable of removing 47.20% (Table S4, ESI†) of the Hg^{II} metal ions from water. Each 2 mL of the **Fmoc-¹Nap-A** hydrogel is capable of removing 208.29 μg of Hg^{II} ions from a total of 440.61 μg of Hg^{II} metal ions contaminated water (Table S4 and Fig. S8, ESI†).

Syneresis of hydrogels in the presence of the thioflavin T (TT) dye. Both **Fmoc-¹Nap-A** and **Fmoc-²Nap-A** hydrogels can absorb the **TT** dye from the water and shrinking of the hydrogels has been observed. It is very important to know the

minimum amount of the **TT** dye required to be added on top of the **Fmoc-¹Nap-A** and **Fmoc-²Nap-A** native hydrogels for syneresis to happen. Both concentration and volume dependent syneresis of **Fmoc-¹Nap-A** and **Fmoc-²Nap-A** hydrogels in the presence of the **TT** dye have been studied to estimate the minimum amount of **TT** dye required for syneresis.

Concentration dependent syneresis of hydrogels in the presence of TT. In this experiment, 1 mL of **TT** dye solution of different concentrations including 1 mg mL^{-1}, 0.1 mg mL^{-1}, 0.01 mg mL^{-1}, and 0.001 mg mL^{-1} has been added on top of four different **Fmoc-¹Nap-A** [2 mL at 0.08% (w/v)] and four different **Fmoc-²Nap-A** hydrogel [2 mL at 0.08% (w/v)] glass vials separately (Fig. 8). Both **Fmoc-¹Nap-A** and **Fmoc-²Nap-A** have absorbed the **TT** dye from all different solutions; however, syneresis has only happened at 1 mg mL^{-1} concentration of **TT** dye.

Volume dependent syneresis of hydrogels in the presence of TT. To measure the minimum volume of **TT** dye solution required for syneresis to happen for **Fmoc-¹Nap-A** and **Fmoc-²Nap-A** hydrogels, 1 mg mL^{-1} **TT** dye solutions with different volumes of 0.1 mL, 0.2 mL, 0.3 mL, 0.4 mL, 0.5 mL, 0.6 mL, 0.7 mL, 0.8 mL, 0.9 mL and 1 mL have been added on top of the **Fmoc-¹Nap-A** [2 mL at 0.08% (w/v)] and **Fmoc-²Nap-A** hydrogel [2 mL at 0.08% (w/v)] vials separately (Fig. 9). All these hydrogel vials have been kept undisturbed under observation to check the syneresis. After five days UV-Vis spectroscopic absorption of the **TT** dye has been recorded by pipetting out the released water from the shrink hydrogels. After five days, absorbance recorded from each vial for the released water by using the UV-Vis spectroscopic study and its concentration have been calculated by using a standard calibration curve of the TT dye (Fig. S9 and S10, ESI†). Fig. S11 (ESI†) shows the UV-Vis absorption profile of the released water from the four different hydrogel vials of **Fmoc-¹Nap-A** shown in Fig. 9.

The UV-Vis absorption spectroscopic profiles of the released water by concentration and volume dependent syneresis of **Fmoc-¹Nap-A** and **Fmoc-²Nap-A** hydrogels are shown in Fig. S11–S14 (ESI†) obtained from Fig. 8 and 9. The volume corrections of the released water have also been considered after syneresis in the calculation. It has been found that the **TT** dye absorption capacity of the **Fmoc-²Nap-A** hydrogel is more than
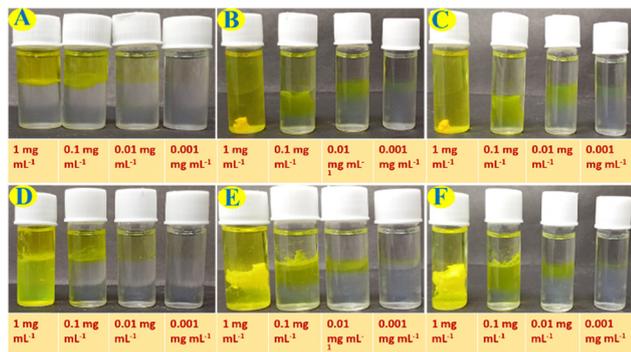
Fig. 8 Concentration dependent syneresis in the presence of the **TT** dye at different time intervals including (A) just after addition, (B) after 3 days and (C) after 5 days for the **Fmoc-¹Nap-A** hydrogel, and (D) just after addition, (E) after 3 days and (F) after 5 days for the **Fmoc-²Nap-A** hydrogel. Concentrations of the **TT** dye added at a volume of 1 mL are mentioned at the bottom of each vial.

that of the **Fmoc-¹Nap-A** hydrogel (Tables S5–S9, ESI†). At the concentrations of 0.001 mg mL^{-1} and 0.01 mg mL^{-1} for dye solutions, both the hydrogels (**Fmoc-¹Nap-A** and **Fmoc-²Nap-A**) have absorbed 100% dye from the solution. The minimum volume of **TT** dye required at a concentration of 1 mg mL^{-1} for the syneresis to happen has been found to be 0.2 mL for the **Fmoc-¹Nap-A** hydrogel [2 mL at 0.08% (w/v)] and 0.3 mL for the **Fmoc-²Nap-A** hydrogel [2 mL at 0.08% (w/v)].

Morphology and structural study of the co-assembled shrink hydrogel matrixes and released water after syneresis induced by metal ions and TT dye

Morphology. To know the morphological nature and obtain detailed structural insight, FE-SEM analysis has been performed for the **Fmoc-¹Nap-A-Hg^{II}** and **Fmoc-¹Nap-A-Ni^{II}** co-assembled shrink hydrogel matrixes and the released water

from the hydrogels after the syneresis (Fig. 10). Nanofibers obtained from the **Fmoc-¹Nap-A-Hg^{II}** shrink hydrogel and released water are of 10.95 ± 1.51 nm and 23.7 ± 3.97 nm in diameter respectively. However, nanofibers obtained from the **Fmoc-¹Nap-A-Ni^{II}** shrink hydrogel and from the released water are of 93.8 ± 25.04 nm and 9.87 ± 1.13 nm in diameter respectively. It has been found that both the shrink hydrogels and the released water consist of nanofibrillar morphology for **Fmoc-¹Nap-A-TT** and **Fmoc-²Nap-A-TT** co-assembled hydrogels (Fig. 11). Nanofibers obtained from the **Fmoc-¹Nap-A-TT** shrink hydrogel and released water are of 10.90 ± 1.49 nm and 205.8 ± 44.01 nm in diameter respectively. However, nanofibers obtained from the **Fmoc-²Nap-A-TT** shrink hydrogel and from the released water are of 19.22 ± 2.37 nm and 22.18 ± 2.06 nm in diameter respectively.

FT-IR analysis

The **Fmoc-¹Nap-A** xerogel's characteristic peaks in the FT-IR spectrum at 3334.92 cm^{-1}, 1691.57 cm^{-1}, 1598.98 cm^{-1}, 1535.33 cm^{-1} for N–H stretching of amide, carbonyl stretching frequency of the amide bond, C=C and N–H bending of the amide group respectively have been observed. However, for the **Fmoc-¹Nap-A-Hg^{II}** matrix, N–H stretching frequency of the amide bond, carbonyl stretching frequency of the amide bond, C=C stretching frequency of the aromatic moiety and N–H bending of the amide bond have been found at 3323.34 cm^{-1}, 1691.57 cm^{-1}, 1597.05 cm^{-1} and 1535.33 cm^{-1} respectively and for the **Fmoc-¹Nap-A-Ni^{II}** matrix N–H stretching frequency of the amide bond, carbonyl stretching frequency of the amide bond, C=C stretching frequency of the aromatic moiety and N–H bending of the amide bond have been found at 3325.27 cm^{-1}, 1693.50 cm^{-1}, 1597.05 cm^{-1} and 1535.33 cm^{-1}

Fig. 9 Volume dependent syneresis in the presence of the **TT** dye at a concentration of 1 mg mL^{-1} at different time intervals including (A) just after addition, (B) after 3 days and (C) after 5 days for the **Fmoc-¹Nap-A** hydrogels, and (D) just after addition, (E) after 3 days and (F) after 5 days for the **Fmoc-²Nap-A** hydrogel. Volume of the **TT** dye added at a concentration of 1 mg mL^{-1} is mentioned at the bottom of each glass vial.
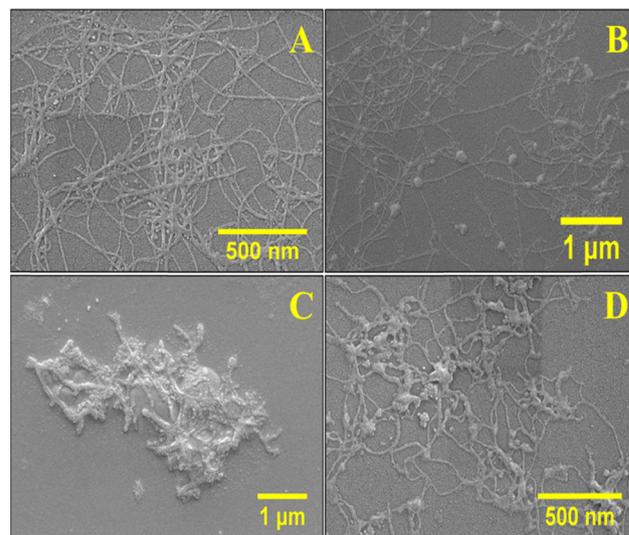

Fig. 10 FE-SEM morphology images of (A) the **Fmoc-¹Nap-A-Hg^{II}** shrink hydrogel matrix, (B) the **Fmoc-¹Nap-A-Ni^{II}** shrink hydrogel matrix, (C) released water after the syneresis from the **Fmoc-¹Nap-A-Hg^{II}** co-assembled hydrogel and (D) released water after the syneresis from the **Fmoc-¹Nap-A-Ni^{II}** co-assembled hydrogel.
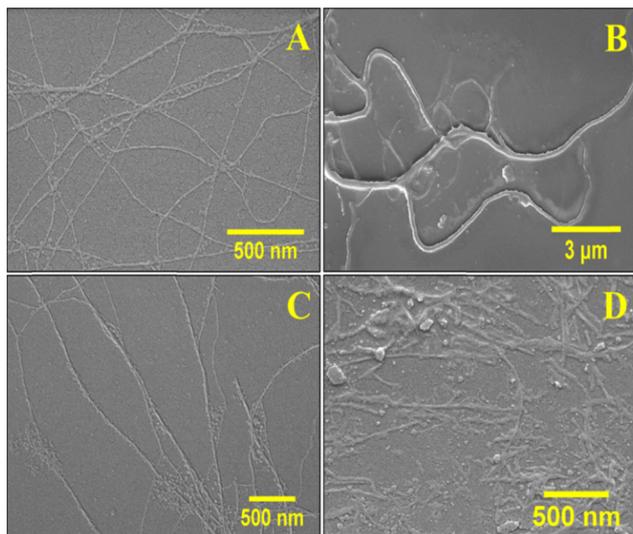
Fig. 11 FE-SEM images of (A) the **Fmoc-¹Nap-A-TT** shrink hydrogel, (B) the released water from the **Fmoc-¹Nap-A-TT** gel matrix, (C) the **Fmoc-²Nap-A-TT** shrink hydrogel, and (D) the released water from the **Fmoc-²Nap-A-TT** gel matrix.

respectively. It has been found that for both **Fmoc-¹Nap-A-Hg^{II}** and **Fmoc-¹Nap-A-Ni^{II}** shrink hydrogel matrixes, the N–H stretching frequencies have changed notably compared to the **Fmoc-¹Nap-A** native xerogel, suggesting hydrogelator–metal ion interactions through amide N–H (Fig. S15, ESI†). Thus, the released water that contains leached hydrogel matrix nanofibers (dissolution) has been more affected due to effective interactions in the solution state over the gel state between the hydrogelator nanofibers and the metal ions (Hg^{II} and Ni^{II}). This may be the probable reason for the destroyed structure of the nanofibers observed in the released water in the presence of metal ions (Hg^{II} and Ni^{II}).

Both the xerogel **Fmoc-¹Nap-A-TT** and **Fmoc-²Nap-A-TT**-matrixes show N–H stretching frequencies of 3334.92 cm^{-1} and 3325.27 cm^{-1} respectively. Other characteristic peaks observed for the **Fmoc-¹Nap-A-TT** matrix include 1691.57 cm^{-1} for the C=O stretching frequency of the amide bond, 1598.98 cm^{-1} for C=C stretching frequency of the aromatic ring, and 1535.35 cm^{-1} for the NH bending of the amide bond. C=O stretching frequency observed at 1691.57 cm^{-1}, C=C stretching frequency of the aromatic ring observed at 1600.91 cm^{-1} and N–H bending of the amide bond observed at 1535.33 cm^{-1} for the **Fmoc-²Nap-A-TT** matrix. The N–H stretching frequencies of both xerogel **Fmoc-¹Nap-A-TT** and **Fmoc-²Nap-A-TT**-matrixes have been red shifted from their native solids (Fig. S3, ESI†). The pure solid **TT** dye shows two characteristic peaks at 1600.91 cm^{-1} and 1504.47 cm^{-1}, for the aromatic moiety (Fig. S15, ESI†). The metal ion (Hg^{II} and Ni^{II})/dye (**TT**)–hydrogelator interaction through amide N–H probably increased the local hydrophobicity of the hydrogels and thus syneresis happened.

X-ray diffraction. X-ray diffraction analysis has been performed for both the **Fmoc-¹Nap-A-Hg^{II}** and **Fmoc-¹Nap-A-Ni^{II}** co-assembled xerogels (freeze-dried shrink gels), which have

been formed after syneresis. Characteristic peaks of the **Fmoc-¹Nap-A-Hg^{II}** matrix have appeared at a d-spacing of 4.89 Å ($2\theta = 18.12°$), representing the hydrogen bonding distance between two adjacent β-strands and also another peak at a d-spacing of 3.83 Å ($2\theta = 23.20°$) that represents the presence of π–π stacking interaction within the hydrogel matrix. However, the characteristic peak at a d-spacing of 4.68 Å ($2\theta = 18.94°$) represents the hydrogen bonding distance between two adjacent β-strands for the **Fmoc-¹Nap-A-Ni^{II}** co-assembled xerogel matrix (Fig. S16, ESI†). The X-ray diffraction study has also been performed on **Fmoc-¹Nap-A-TT** and **Fmoc-²Nap-A-TT** xerogels. The **Fmoc-¹Nap-A-TT** xerogel shows characteristic peaks at $d = 9.33$ Å ($2\theta = 9.47°$), $d = 4.67$ Å ($2\theta = 18.96°$) and $d = 3.81$ Å ($2\theta = 23.28°$). The **Fmoc-²Nap-A-TT** matrix also shows these three characteristic peaks at the same d spacing and 2θ values. The distance between two neighbouring layers of the beta-sheet indicated by the d-spacing value of 9.33 Å and d-spacing value of 4.67 Å represents the hydrogen bonding distance between two adjacent β-strands. Also, the presence of π–π stacking interaction has been confirmed by the peak, at a d-spacing of 3.81 Å ($2\theta = 23.28°$) (Fig. S16, ESI†).

Effect of other metal ions on Fmoc-¹Nap-A and Fmoc-²Nap-A hydrogels

Syneresis of the hydrogels **Fmoc-¹Nap-A** and **Fmoc-²Nap-A** has also been tested in the presence of 20 mg mL^{-1} of different metal salts including AgNO$_3$ (A), BaCl$_2$ (B), CaCl$_2$ (C), Cd(OAc)$_2$ (D), Co(NO$_3$)$_2$ (E), CuSO$_4$ (F), FeSO$_4$ (G), Hg(OAc)$_2$ (H), HgCl$_2$ (I), K$_2$CrO$_4$ (J), KBr (K), MgSO$_4$ (L), NaCl (M), NaOAc (N), NiCl$_2$ (O), Pb(OAc)$_2$ (P), and ZnSO$_4$ (Q). The fate of both **Fmoc-¹Nap-A** and **Fmoc-²Nap-A** hydrogels in the presence of 20 mg mL^{-1} of different metal salts is shown in Fig. S17 and S18 (ESI†). It was found that only the **Fmoc-¹Nap-A** hydrogel showed syneresis in the presence of Hg(OAc)$_2$, HgCl$_2$, and NiCl$_2$ selectively. No syneresis has been observed for **Fmoc-¹Nap-A** and **Fmoc-²Nap-A** hydrogels in the presence of other metal ions.

Biological evaluation

Agar disk diffusion method. The antibacterial activity of hydrogels **Fmoc-¹Nap-A** and **Fmoc-²Nap-A** has been evaluated using the agar disk diffusion assay against both Gram-positive bacteria (*S. aureus* and *E. faecalis*) and Gram-negative bacteria (*P. aeruginosa* and *K. pneumoniae*). The results reveal distinct differences in the efficacy of the hydrogels, both across different bacterial strains and between the two types of hydrogels as shown in Fig. 12. For Gram-positive bacteria, *S. aureus* and *E. faecalis*, the positive controls linezolid and ampicillin both demonstrated inhibition zones of 20 mm, demonstrating strong antibacterial activity (Table S10, ESI†). Hydrogel **Fmoc-¹Nap-A** exhibited considerable antibacterial activity against these strains, with inhibition zones of 18 ± 2 mm for *S. aureus* and 16 ± 2 mm for *E. faecalis*, suggesting that **Fmoc-¹Nap-A** is fairly effective against Gram-positive bacteria, though slightly less than the respective antibiotics. In contrast, **Fmoc-²Nap-A** displayed markedly lower activity, with inhibition zones of 10 ± 1 mm against *S. aureus* and 11 ± 1 mm against *E. faecalis*,
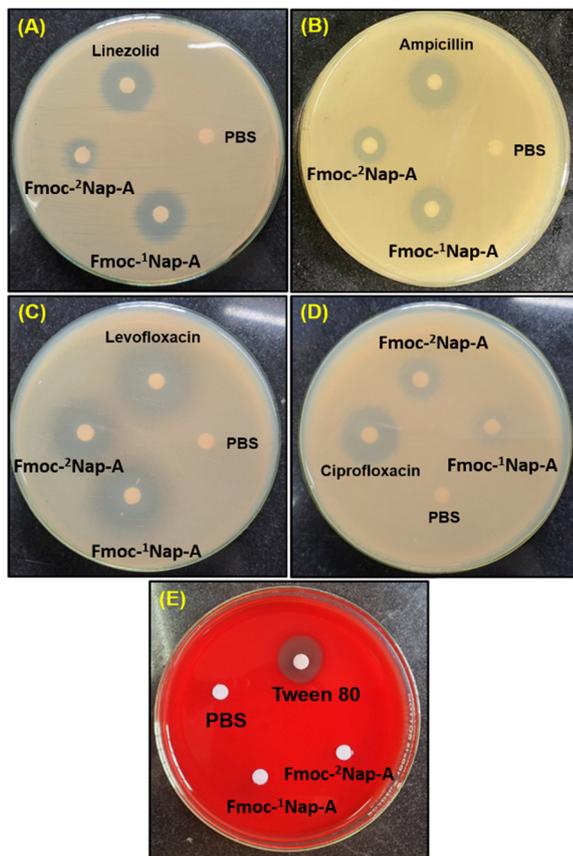
Fig. 12 Antibacterial and hemolytic activity of the prepared hydrogels *i.e.*, **Fmoc-¹Nap-A** [1% (w/v), 2.2 mM] and **Fmoc-²Nap-A** [1% (w/v), 2.2 mM]. Disk diffusion assay showing antibacterial activity against (A) *Staphylococcus aureus* (ATCC 25923) with linezolid as the positive control; (B) *Enterococcus faecalis* (ATCC 29212) with ampicillin as the positive control; (C) *Pseudomonas aeruginosa* (ATCC 27853) with levofloxacin as the positive control; and (D) *Klebsiella pneumoniae* (ATCC 13883) with ciprofloxacin as the positive control. PBS served as the negative control. (E) Hemolytic assay on a blood agar plate showing no hemolysis by hydrogels **Fmoc-¹Nap-A** and **Fmoc-²Nap-A**, with Tween 80 as the positive control and PBS as the negative control.

Fmoc-¹Nap-A and **Fmoc-²Nap-A** could be attributed to variations in their chemical composition or structural properties, which may influence their ability to penetrate bacterial cell walls or disrupt bacterial processes. The stronger antibacterial efficacy of **Fmoc-¹Nap-A** against both Gram-positive and Gram-negative bacteria suggests that it may possess more favorable physicochemical characteristics that enhance its antibacterial efficacy. Gram-positive bacteria, with their thicker peptidoglycan layer,[64] tend to be more susceptible to antibacterial agents that can disrupt cell wall synthesis, which might explain the effectiveness of **Fmoc-¹Nap-A**. On the other hand, Gram-negative bacteria possess an additional outer membrane that acts as a barrier to many antibiotics, making them more resistant;[65] however, the ability of **Fmoc-¹Nap-A** to inhibit *P. aeruginosa* suggests that it may have mechanisms that enable it to overcome this barrier to some extent. Therefore, the promising antibacterial activity of hydrogel **Fmoc-¹Nap-A**, particularly against *P. aeruginosa* and *S. aureus*, makes it a potential candidate for further development as an antibacterial agent.

Hemolytic assay

The hemolytic activity of hydrogels **Fmoc-¹Nap-A** and **Fmoc-²Nap-A** has been assessed using a blood agar plate, alongside positive and negative controls, Tween 80 and PBS, respectively to assess their potential cytotoxicity towards erythrocytes. The results demonstrated that Tween 80 used as the positive control exhibited a clear zone of hemolysis, confirming its cytotoxic nature. In contrast, PBS as the negative control showed no hemolysis validating its non-hemolytic nature. Both hydrogels, **Fmoc-¹Nap-A** and **Fmoc-²Nap-A**, displayed no visible hemolysis on the blood agar plate, suggesting that neither hydrogel induces red blood cell lysis (Fig. 12). This lack of hemolysis confirms the biocompatibility of **Fmoc-¹Nap-A** and **Fmoc-²Nap-A**, making them suitable candidates for biomedical applications where non-cytotoxicity is crucial, such as in wound dressings or drug delivery systems. The non-hemolytic nature of these hydrogels, combined with the previously observed
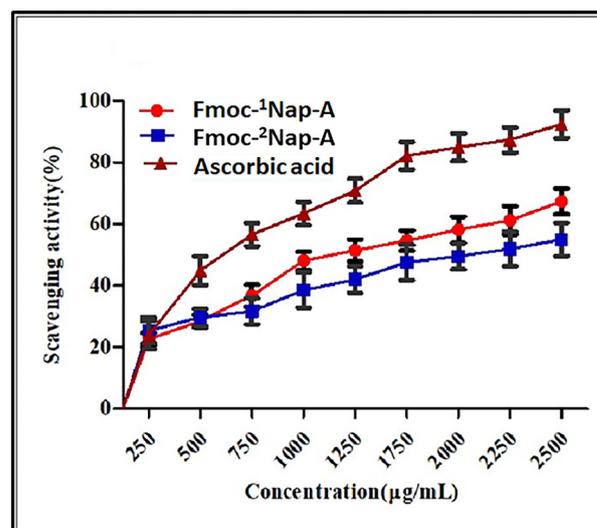
indicating a weaker antibacterial effect. In the case of Gram-negative bacteria, the treatment is more challenging due to the presence of an outer membrane, which often confers resistance to many antibiotics (Fig. 12).[64,65]

Against *P. aeruginosa* and *K. pneumoniae*, the positive controls levofloxacin and ciprofloxacin exhibited inhibition zones of 27 ± 1 mm and 21 ± 1 mm, respectively. In comparison, **Fmoc-¹Nap-A** showed strong antibacterial activity against *P. aeruginosa*, with an inhibition zone of 24 ± 1 mm, approaching the efficacy of levofloxacin. However, its activity against *K. pneumoniae* was significantly less, with an inhibition zone of 11 ± 2 mm. **Fmoc-²Nap-A**; while less effective than **Fmoc-¹Nap-A**, it still showed better antibacterial activity, with inhibition zones of 21 ± 2 mm for *P. aeruginosa* while poor activity with an inhibition zone of 8 ± 1 mm for *K. pneumoniae*. The blood agar shows no hemolysis by **Fmoc-¹Nap-A** and **Fmoc-²Nap-A** hydrogels, with Tween 80 as the positive control, and PBS as the negative control. The difference in antibacterial activity between

Fig. 13 Graphical representation of antioxidant assay of hydrogels **Fmoc-¹Nap-A** and **Fmoc-²Nap-A**.

antibacterial efficacy of **Fmoc-¹Nap-A**, further supports their potential for safe and effective use in clinical settings.

Antioxidant assay

This is the most commonly used method for estimating anti-oxidant activity, where DPPH changes from purple to yellow, indicating the scavenging properties of the synthesized compound.[66] In the DPPH assay, the purple DPPH radical is reduced when an antioxidant donates a hydrogen atom or electron, neutralizing it and forming a non-radical compound (DPPH-H). This reaction results in a color change from purple to yellow. The decrease in color intensity, measured at 517 nm, is directly correlated with the antioxidant's radical scavenging capability. The positive and negative control used were methanol and ascorbic acid, whereas the hydrogels of both **Fmoc-¹Nap-A** and **Fmoc-²Nap-A** were both evaluated at concentrations of 250 $\mu g\ mL^{-1}$, 500 $\mu g\ mL^{-1}$, 750 $\mu g\ mL^{-1}$, 1000 $\mu g\ mL^{-1}$, 1250 $\mu g\ mL^{-1}$, 1500 $\mu g\ mL^{-1}$, 1750 $\mu g\ mL^{-1}$, 2000 $\mu g\ mL^{-1}$, 2250 $\mu g\ mL^{-1}$, and 2500 $\mu g\ mL^{-1}$ for the antioxidant potential. The hydrogels **Fmoc-¹Nap-A** and **Fmoc-²Nap-A** both demonstrated effective antioxidant activity, with **Fmoc-¹Nap-A** having a scavenging activity of 67% and **Fmoc-²Nap-A** having a scavenging activity of 54% while comparing it with ascorbic acid having 88%. The results are summarized in Fig. 13. Hydrogels **Fmoc-¹Nap-A** and **Fmoc-²Nap-A** showed 50% scavenging activity at 1000 $\mu g\ \mu L^{-1}$ and 2000 $\mu g\ mL^{-1}$ respectively, whereas comparing it with ascorbic acid showed 50% scavenging activity at 750 $\mu g\ mL^{-1}$. The antioxidant properties of the compound depend on its reducing capability; hydrogel **Fmoc-¹Nap-A** has the best antioxidant potential as it reduces the free radical to the greatest extent, while the compound **Fmoc-²Nap-A** has demonstrated promising antioxidant potential.

Effect of the compounds on the proliferation of pancreatic cancer cells

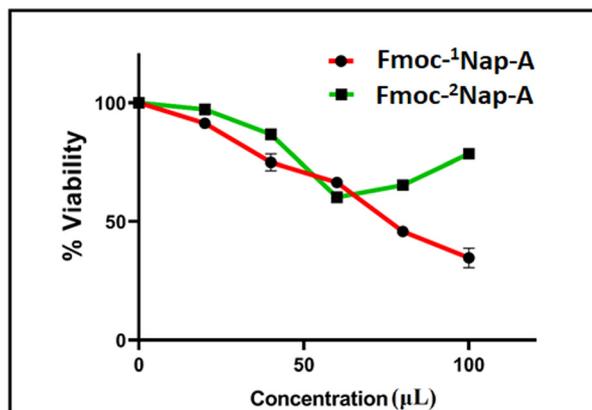To determine if the compounds had elicited any cytotoxic effect in pancreatic cancer cells, an MTT assay has been performed using PANC-1 cell lines. The individual IC$_{50}$ values of the compounds **Fmoc-¹Nap-A** and **Fmoc-²Nap-A** were 77.97 μL and 145.51 μL, respectively. Among the compounds, **Fmoc-¹Nap-A** displayed the most potent minimal effective concentration at an average of 77. 97 μL (Fig. 14). However, **Fmoc-²Nap-A** depicted only a moderate anti-proliferative effect with the highest minimal IC$_{50}$ value (Fig. 14).

Effect of the compounds on the morphology of pancreatic cancer cells

To elucidate if the growth-inhibitory effect observed by the cell viability assay was due to the induction of apoptosis, AO/EB dual staining has been performed. Following staining, it has been observed that about 95% of the control cells were spindle-shaped, emitting green fluorescence with clear demarcation and whole nucleus (Fig. 15). Upon exposure to the compounds, a gradual reduction in the percentage of viable cells (emitting green fluorescence) with a concomitant increase in the apoptotic cells (emitting orange-red fluorescence) has been observed. Markedly, among the treatment groups employed, **Fmoc-¹Nap-A** depicted a significant increase in the number of apoptotic cells, with approximately 64% of apoptotic bodies emitting orange-red EB fluorescence when compared with **Fmoc-²Nap-A** and the mock group ($p < 0.001$) (Fig. 15). However, about 72% of the cells treated with **Fmoc-²Nap-A** portrayed a green fluorescence (Fig. 15). Overall, the AO/EB staining results suggested that the compound **Fmoc-¹Nap-A** was more effective in the morphological induction of apoptosis in the chosen pancreatic cancer cell line.
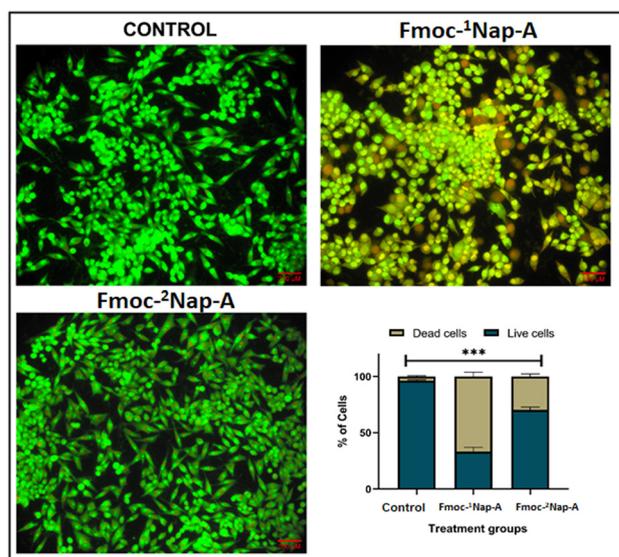

Fig. 14 Cytotoxicity analysis of PANC-1 cells treated with the compounds **Fmoc-¹Nap-A**, and **Fmoc-²Nap-A**, wherein **Fmoc-¹Nap-A** had sensitized the pancreatic cancer cells more effectively with an IC$_{50}$ value of 77.97 μL. Data are expressed as mean $\pm$ SD of three independent experiments, $n = 3$.

Fig. 15 PANC-1 cells treated with **Fmoc-¹Nap-A** and **Fmoc-²Nap-A** were stained with AO/EB. Morphological changes in the cells following exposure to the compounds were identified at $20\times$ magnification by fluorescence microscopy. Quantitative data of fluorescence intensities were obtained using Fiji software, ***$p < 0.001$ when compared with the control, $n = 3$.

Conclusion

Fmoc-¹Nap-A and **Fmoc-²Nap-A** form stable hydrogels in 50 mM phosphate buffer of pH 7.4. External stimuli responsive syneresis in the presence of Hg^{II} and Ni^{II} metal ions for the **Fmoc-¹Nap-A** hydrogel and thioflavin T induced syneresis for both the **Fmoc-¹Nap-A** and **Fmoc-²Nap-A** hydrogels have been selectively reported in this study. This study reveals that the **Fmoc-¹Nap-A** hydrogel can remove toxic heavy Hg^{II} metal ions through absorption of metal ions within the gel matrix followed by syneresis induced by a high amount of toxic Hg^{II} metal ions containing waste-water effectively. ICP-MS data show the effectiveness of this toxic metal ion removal by the **Fmoc-¹Nap-A** hydrogel. Both the **Fmoc-¹Nap-A** and **Fmoc-²Nap-A** hydrogels can absorb thioflavin T very efficiently from dye contaminated waste-water in the gel matrix and release almost pure water by the syneresis effect. **Fmoc-²Nap-A** shows higher efficiency for the removal of the **TT** dye from the water compared to **Fmoc-¹Nap-A**. The MTT study shows that both the hydrogels are biocompatible and show anticancer activity toward the pancreatic cancer cell line. Both of these hydrogels show potent anti-bacterial and anti-oxidant properties. All of these experiments uphold the importance of supramolecular chemistry and gelation study, where weak interactions including pi–pi stacking, hydrogen bonding and indeed hydrophobic interactions play key roles in hydrogelation followed by external stimuli responsive syneresis, suggesting application in environmental remediation. The presence of high content of Hg^{II} toxic metal ions and toxic dyes in waste-water can be detected by using these hydrogels and their corresponding water treatment can be performed to get clean water following green and sustainable pathways.

Author contributions

All authors have approved the final version of the manuscript. A. B. was responsible for the hydrogelation, methodology, investigations, characterization, graph preparation from raw data and their calculations, writing the early-stage draft, and formatting. R. R. P. was responsible for performing antibacterial, hemolytic, and antioxidant studies. S. D. P. was responsible for the MTT assay and cell line studies. M. S. was responsible for the supervision of the antibacterial, hemolytic, and antioxidant studies and this part writing. B. A. K. and S. B. were responsible for the supervision and the writing of the MTT assay and cell line studies. M. V. was responsible for the rheological measurements. S. R. was responsible for conceptualization, supervision, writing of the manuscript, review, editing, and finalization of the manuscript and ESI.†

Data availability

The data used to support this study findings are included within the paper and in the supplementary information file (ESI†).

Conflicts of interest

The authors declare there are no conflicts of interest.

Acknowledgements

Notes and references

1 C. Ren, L. Chu, F. Huang, L. Yang, H. Fan, J. Liu and C. Yang, *RSC Adv.*, 2017, **7**, 1313–1317.
2 H. Najafi, A. M. Tamaddon, S. Abolmaali, S. Borandeh and N. Azarpira, *Soft Matter*, 2021, **17**, 57–67.
3 J. E. P. Sun, B. Stewart, A. Litan, S. J. Lee, J. P. Schneider, S. A. Langhans and D. J. Pochan, *Biomater. Sci.*, 2016, **4**, 839–848.
4 B. Mondal, V. K. Gupta, B. Hansda, A. Bhoumik, T. Mondal, H. K. Majumder, C. J. C. Edwards-Gayle, I. W. Hamley, P. Jaisankar and A. Banerjee, *Soft Matter*, 2022, **18**, 7201–7216.
5 R. Huang, W. Qi, L. Feng, R. Su and Z. He, *Soft Matter*, 2011, **7**, 6222–6230.
6 K. Gayen, K. Basu, D. Bairagi, V. Castelletto, I. W. Hamley and A. Banerjee, *ACS Appl. Bio Mater.*, 2018, **1**, 1717–1724.
7 T. De Serres-Bérard, T. B. Becher, C. B. Braga, C. Ornelas and F. Berthod, *ACS Appl. Polym. Mater.*, 2020, **2**, 5790–5797.
8 L. Wang, J. Li, Y. Xiong, Y. Wu, F. Yang, Y. Guo, Z. Chen, L. Gao and W. Deng, *ACS Appl. Mater. Interfaces*, 2021, **13**, 58329–58339.
9 M. Criado-Gonzalez, E. Espinosa-Cano, L. Rojo, F. Boulmedais, M. R. Aguilar and R. Hernández, *ACS Appl. Mater. Interfaces*, 2022, **14**, 10068–10080.
10 Q. Zhao, Y. Zhao, Z. Lu and Y. Tang, *ACS Appl. Mater. Interfaces*, 2019, **11**, 16320–16327.
11 S. R. Nelli, R. D. Chakravarthy, M. Mohiuddin and H.-C. Lin, *RSC Adv.*, 2018, **8**, 14753–14759.
12 R. Bassan, M. Varshney and S. Roy, *ChemistrySelect*, 2023, **8**, e202203317.
13 S.-Y. Qin, Y. Pei, X.-J. Liu, R.-X. Zhou and X.-Z. Zhang, *J. Mater. Chem. B*, 2013, **1**, 668–675.
14 I. Maity, T. K. Mukherjee and A. K. Das, *New J. Chem.*, 2014, **38**, 376–385.
15 J. Nanda, B. Adhikari, S. Basak and A. Banerjee, *J. Phys. Chem. B*, 2012, **116**, 12235–12244.
16 B. Adhikari and A. Banerjee, *Soft Matter*, 2011, **7**, 9259–9266.
17 D. M. Ryan, S. B. Anderson and B. L. Nilsson, *Soft Matter*, 2010, **6**, 3220–3231.

18 W. Zhang, K. Zhang, S. Yan, J. Wu and J. Yin, *J. Mater. Chem. B*, 2018, **6**, 6865–6876.

19 Y. Zhu, L. Wang, Y. Li, Z. Huang, S. Luo, Y. He, H. Han, F. Raza, J. Wu and L. Ge, *Biomater. Sci.*, 2020, **8**, 5415–5426.

20 R. Liang, Z. Luo, G. Pu, W. Wu, S. Shi, J. Yu, Z. Zhang, H. Chen and X. Li, *RSC Adv.*, 2016, **6**, 76093–76098.

21 M. L. Jagrosse, P. Agredo, B. L. Abraham, E. S. Toriki and B. L. Nilsson, *ACS Biomater. Sci. Eng.*, 2023, **9**, 784–796.

22 B. L. Abraham, E. S. Toriki, N. J. Tucker and B. L. Nilsson, *J. Mater. Chem. B*, 2020, **8**, 6366–6377.

23 A. Baral, S. Roy, A. Dehsorkhi, I. W. Hamley, S. Mohapatra, S. Ghosh and A. Banerjee, *Langmuir*, 2014, **30**, 929–936.

24 H. Vilaça, T. Castro, F. M. G. Costa, M. Melle-Franco, L. Hilliou, I. W. Hamley, E. M. S. Castanheira, J. A. Martins and P. M. T. Ferreira, *J. Mater. Chem. B*, 2017, **5**, 8607–8617.

25 K. Ghosh and S. Panja, *ChemistrySelect*, 2016, **1**, 3667–3674.

26 D. Ghosh, D. Deepa and K. K. Damodaran, *Supramol. Chem.*, 2020, **32**, 276–286.

27 K. Ghosh, S. Panja and S. Bhattacharya, *RSC Adv.*, 2015, **5**, 72772–72779.

28 Y. Zhang, Y.-C. Pan, Y. Wang, D.-S. Guo, J. Gao and Z. Yang, *Nanoscale*, 2018, **10**, 18829–18834.

29 S. Basak, N. Nandi, S. Paul, I. W. Hamley and A. Banerjee, *Chem. Commun.*, 2017, **53**, 5910–5913.

30 B. Mondal, D. Bairagi, N. Nandi, B. Hansda, K. S. Das, C. J. C. Edwards-Gayle, V. Castelletto, I. W. Hamley and A. Banerjee, *Langmuir*, 2020, **36**, 12942–12953.

31 Z. Li, Z. Luo, J. Zhou, Z. Ye, G.-C. Ou, Y. Huo, L. Yuan and H. Zeng, *Langmuir*, 2020, **36**, 9090–9098.

32 M. Abbas, H. H. Susapto and C. A. E. Hauser, *ACS Omega*, 2022, **7**, 2082–2090.

33 S. Roy and A. Banerjee, *Soft Matter*, 2011, **7**, 5300–5308.

34 M. Criado-Gonzalez, J. Rodon Fores, A. Carvalho, C. Blanck, M. Schmutz, L. Kocgozlu, P. Schaaf, L. Jierry and F. Boulmedais, *Langmuir*, 2019, **35**, 10838–10845.

35 B. Das Gupta, A. Halder, T. Vijayakanth, N. Ghosh, R. Konar, O. Mukherjee, E. Gazit and S. Mondal, *J. Mater. Chem. B*, 2024, **12**, 8444–8453.

36 A. Baral, S. Roy, S. Ghosh, D. Hermida-Merino, I. W. Hamley and A. Banerjee, *Langmuir*, 2016, **32**, 1836–1845.

37 A. P. McCloskey, M. Lee, J. Megaw, J. McEvoy, S. M. Coulter, S. Pentlavalli and G. Laverty, *ACS Omega*, 2019, **4**, 2584–2589.

38 F. Cao, G. Ma, M. Song, G. Zhu, L. Mei and Q. Qin, *Soft Matter*, 2021, **17**, 4445–4451.

39 S. Roy, D. K. Maiti, S. Panigrahi, D. Basak and A. Banerjee, *RSC Adv.*, 2012, **2**, 11053–11060.

40 R. Bassan, B. Mondal, M. Varshney and S. Roy, *Nanoscale Adv.*, 2024, **6**, 3399–3409.

41 I. Maity, D. B. Rasale and A. K. Das, *Soft Matter*, 2012, **8**, 5301–5308.

42 D. K. K. Kori, T. Ghosh and A. K. Das, *Catal. Sci. Technol.*, 2023, **13**, 2540–2550.

43 J. Wang, H. Wang, Z. Song, D. Kong, X. Chen and Z. Yang, *Colloids Surf., B*, 2010, **80**, 155–160.

44 S. Kiyonaka, K. Sugiyasu, S. Shinkai and I. Hamachi, *J. Am. Chem. Soc.*, 2002, **124**, 10954–10955.

45 Z. Azoulay and H. Rapaport, *J. Mater. Chem. B*, 2016, **4**, 3859–3867.

46 D. K. Duraisamy, P. D. Sureshbhai, P. Saveri, A. P. Deshpande and G. Shanmugam, *Chem. Commun.*, 2022, **58**, 13377–13380.

47 T. Divoux, B. Maoa and P. Snabre, *Soft Matter*, 2015, **11**, 3677–3685.

48 M. P. Conte, N. Singh, I. R. Sasselli, B. Escuder and R. V. Ulijn, *Chem. Commun.*, 2016, **52**, 13889–13892.

49 L. Qin, P. Duan, F. Xie, L. Zhang and M. Liu, *Chem. Commun.*, 2013, **49**, 10823–10825.

50 B. K. Das, B. Pramanik, S. Chowdhuri, O. A. Scherman and D. Das, *Chem. Commun.*, 2020, **56**, 3393–3396.

51 S. Panja, B. Dietrich and D. J. Adams, *Angew. Chem., Int. Ed.*, 2022, **61**, e202115021.

52 T. Sugiura, T. Kanada, D. Mori, H. Sakai, A. Shibata, Y. Kitamura and M. Ikeda, *Soft Matter*, 2020, **16**, 899–906.

53 D. J. Adams, L. M. Mullen, M. Berta, L. Chen and W. J. Frith, *Soft Matter*, 2010, **6**, 1971–1980.

54 A. M. Castilla, M. Wallace, L. L. E. Mears, E. R. Draper, J. Doutch, S. Rogers and D. J. Adams, *Soft Matter*, 2016, **12**, 7848–7854.

55 S. C. Lange, J. Unsleber, P. Drücker, H.-J. Galla, M. P. Waller and B. J. Ravoo, *Org. Biomol. Chem.*, 2015, **13**, 561–569.

56 F. Xie, L. Qin and M. Liu, *Chem. Commun.*, 2016, **52**(5), 930–933.

57 M. Bastrop, A. Meister, H. Metz, S. Drescher, B. Dobner, K. Mäder and A. Blume, *J. Phys. Chem. B*, 2011, **115**(1), 14–22.

58 B. D. Pinto, O. Ronsin and T. Baumberger, *Soft Matter*, 2023, **19**, 1720–1731.

59 Y. Ma, B. Li, K. Zhang, Q. Wan, Z. Džolić and B. Z. Tang, *J. Mater. Chem. C*, 2020, **8**, 13705–13712.

60 J. Liu, F. Yin, J. Hu and Y. Ju, *Mater. Chem. Front.*, 2021, **5**(16), 4764–4771.

61 F. Li, L. Gao, X. Zhang, P. Wang, Y. Liu, J. Feng, C. Zhang, C. Zhao and S. Zhang, *Nanoscale Adv.*, 2021, **3**, 6056–6062.

62 L. Zhu, C. Yang and J. Qin, *Chem. Commun.*, 2008, 6303–6305.

63 M. Más-Montoya and R. A. J. Janssen, *Adv. Funct. Mater.*, 2017, **27**, 1605779.

64 G. K. Auer and D. B. Weibel, *Biochemistry*, 2017, **56**(29), 3710–3724.

65 Z. Breijyeh, B. Jubeh and R. Karaman, *Molecules*, 2020, **25**(6), 1340.

66 M. Javaid, I.-U. Haq, H. Nadeem, H. Fatima, A.-U. Khan and N. Irshad, *Front. Pharmacol.*, 2023, **14**, 1084181.